International Journal of Coal Geology 163 (2016) 177–185

Contents lists available at ScienceDirect

International Journal of Coal Geology

journal homepage: www.elsevier.com/locate/ijcoalgeo

The effect of sample particle size on the determination of pore structure parameters in shales

Mingming Wei, Yongqiang Xiong *, Li Zhang, Jinhua Li, Ping'an Peng

State Key Laboratory of Organic Geochemistry, Guangzhou Institute of Geochemistry of CAS, Guangzhou 510640, China

ARTICLE INFO

Article history:
Received 8 October 2015
Received in revised form 17 July 2016
Accepted 21 July 2016
Available online 25 July 2016

Keywords:
Shale
Sample particle size
Pore structure
N_2 and CO_2 low-pressure adsorption
60–140 mesh

ABSTRACT

The combination of low-pressure N_2 and CO_2 adsorption could provide an effective approach for characterizing the pore structure of shales. Although gas adsorption methods generally do not destroy the pore structure during experimental process, sample particle sizes could significantly affect experimental results that can approach or deviate from the real value. Therefore, the determination of pore structure is closely related to the sample particle size. In the current study, 4 fresh core samples of different compositions and total organic carbon (TOC) ranges collected from the Sichuan Basin were analyzed to elucidate the effect of sample particle size on the determination of pore structure parameters. Samples were ground and then sieved into seven groups based on particle size ranges, i.e., <60, 60–80, 80–100, 100–120, 120–140, 140–200 and >200 mesh, for measurements of low-pressure N_2 and CO_2 adsorption, TOC contents, and X-ray diffraction (XRD) mineralogy.

TOC results show a slight enrichment whereas XRD minerals vary irregularly, with sample particle size decreases. Meanwhile, the TOC and mineral contents show insignificant statistical relation with pore structure parameters in all sample particle size ranges. Therefore, variations in organic matter content and mineral composition that result from sieving are unlikely to have a significant influence on the pore structure of shale. Rather, sample particle size may be the most important control on pore structure characteristics in the samples analyzed in this study.

The relative standard deviations (RSDs) for Brunauer–Emmett–Teller (BET) N_2 surface areas, Dubinin–Radushkevich (D–R) CO_2 micropore surface areas and non-local density functional theory (NLDFT) N_2 and CO_2 nanopore surface areas measurements are <5%, within analytical error. Therefore, in the studied grain size range (60–200 mesh), the sample particle size shows insignificant effects on surface area results. However, samples with smaller particle size have a greater effect on pore volume and pore size, especially for pore size distribution (PSD) of N_2 low-pressure adsorption. The RSDs of the Barrett–Joyner–Halenda (BJH) pore volumes and BET pore sizes of all samples in the 140–200 mesh range are obviously greater than the values of other mesh ranges. Moreover, in the dV/dlogw plots of PSD analysis, high N_2 peaks and new N_2 peaks appeared in the 10–100 nm pore-width range, particularly for samples in the >140 mesh range. The 60–140 mesh particle-size range is therefore recommended for N_2 low-pressure adsorption. Finally, the sample particle size has insignificant effect on the pore system parameters for grains in the 60–200 mesh range for CO_2 low-pressure adsorption. Overall, the results confirm that the 60–140 mesh particle-size range can be used for both N_2 and CO_2 low-pressure adsorption measurements.

1. Introduction

Natural gas may be stored in organic-rich shales as a combination of free gas, adsorbed gas and dissolved gas (Curtis, 2002; Ross and Bustin, 2009). Shales are generally characterized by low porosity and permeability, and shale gas production depends on the ability of pore systems to store and release hydrocarbon gas. Pore system characterization is therefore an important step in the evaluation of shale gas reservoirs. To improve our understanding of the relationship between a given pore system and gas storage capacity, various techniques (e.g., organic petrology, CO_2 and N_2 low-pressure adsorption, and high-pressure mercury intrusion) are used to quantify the surface area, pore volume, pore size, and pore size distribution of the shale.

Low-pressure gas adsorption is an important approach for characterizing the pore systems of shale samples, i.e., surface area and microporosity. Factors that may influence these measurements include pore size, particle size, and surface roughness (Jiang et al., 2014; Tsai, 2013). Although pore size is the most important factor, gas adsorption methods generally do not destroy the pore size during experimental process, while the surface area of shale may be closely related to particle size and surface roughness. Furthermore, surface roughness has little

* Corresponding author.
E-mail address: xiongyq@gig.ac.cn (Y. Xiong).

http://dx.doi.org/10.1016/j.coal.2016.07.013
0166-5162/

difference in the same sample preparation techniques. Therefore, the determination of pore structure is closely related to the sample particle size, and particle sizes could significantly affect experimental results that can approach or deviate from the real value. Despite the microstructural data of shale sample are growing (e.g., Ross and Bustin, 2007; Chalmers et al., 2012; Clarkson et al., 2013; Tan et al., 2014a, 2014b; Tian et al., 2015), a unified standard for sample particle size has not been adopted among the various low-pressure adsorption experimental methods. For example, in China, samples are generally ground to a maximum particle size of 100 mm, as outlined in the National Standards of the People's Republic of China (GB/T 21650.2-2008 and GB/T 21650.3-2011). Other studies report that samples were ground to grain sizes of 1–2 mm (Hou et al., 2014) or other millimeter-size particles (Clarkson et al., 2012). Tian et al. (2013, 2015) ground shale samples into grains of 60–80 mesh (250–180 μm) and 60–100 mesh (250–150 μm), and Zelenev et al. (2011) ground samples to 40 mesh (<380 μm). Many researchers ground samples so they pass through a 60 mesh sieve (<250 μm) (Chalmers and Bustin, 2007; Ross and Bustin, 2007, 2009; Chalmers et al., 2012; Clarkson et al., 2013; Labani et al., 2013; Lahann et al., 2013; Wang et al., 2014). However, in other studies samples have been ground to 70 mesh (<200 μm; Tan et al., 2014a, 2014b; Yang et al., 2014), 80 mesh (<180 μm; Guo et al., 2014), and 100 mesh (<150 μm; Wang et al., 2013; Cao et al., 2015). Furthermore, other studies did not explicitly state the sample particle size when conducting low-pressure adsorption measurements (Busch et al., 2008; Chareonsuppanimit et al., 2012; Ji et al., 2012; Han et al., 2013; Liu et al., 2013; Mastalerz et al., 2013; Chen and Xiao, 2014; Yuan et al., 2014; Li et al., 2015). It is therefore difficult to compare the pore structural data of different laboratories.

In the current research, we aim to evaluate the effect of sample particle size on the determination of specific surface area, pore volume, pore size and pore size distribution in shale samples, and to propose a suitable particle-size range for low-pressure N_2 and CO_2 adsorption measurements.

2. Samples and experimental methods

2.1. Sample preparation

Four fresh core samples of different compositions and TOC ranges from the large-scale development shale gas fields of China were collected and analyzed in this study. The measured samples are black shales deposited in marine environments from Sichuan Basin located in the northwest part of the Upper Yangtze Platform, South China (Fig. 1) (Tan et al., 2013, 2015). The organic rich lower Silurian Longmaxi shale formation is widely present in the basin, and the principal rock types are black carbonaceous and siliceous shale that is rich in organic matter, mudstone and siltstone (Fig. 2). This formation has been identified as an important target for shale gas exploration (Wang et al., 2013; Tan et al., 2014a, 2014b, 2015).

Prior to analysis, the samples were cut into fragments of ~10 mm, and then ground for ~30 s in a Mini Superfine Mill. The ground samples were sieved into seven particle-size ranges: <60, 60–80, 80–100, 100–120, 120–140, 140–200, and >200 mesh. The mass fraction of each particle-size range is listed in Table 1. The groups with a sample particle size larger than 200 or <60 mesh were not analyzed because of the mass range limitation.

2.2. Total organic carbon (TOC) content and X-ray diffraction (XRD) analysis

The behavior of shale as a reservoir rock for gas is influenced not only by storage mechanisms, which are controlled by mineral content (Bruant et al., 2002), but also, and more importantly, by the characteristics of organic matter that offers sorption sites on the organic surface area of mesopores or volume filling in micropores (Clarkson et al., 2013). Therefore, it is necessary to determine the TOC content and mineral composition for different particle sizes.

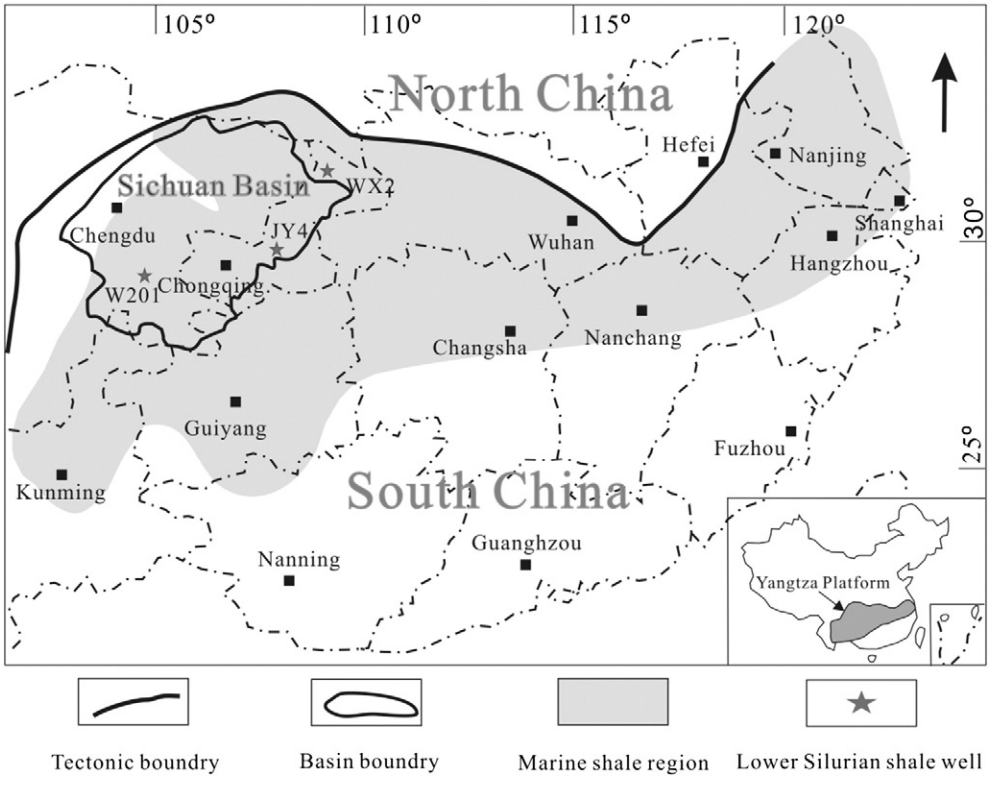

Fig. 1. Locations of the sampled wells in Sichuan Basin of the Upper Yangtze Platform, South China.

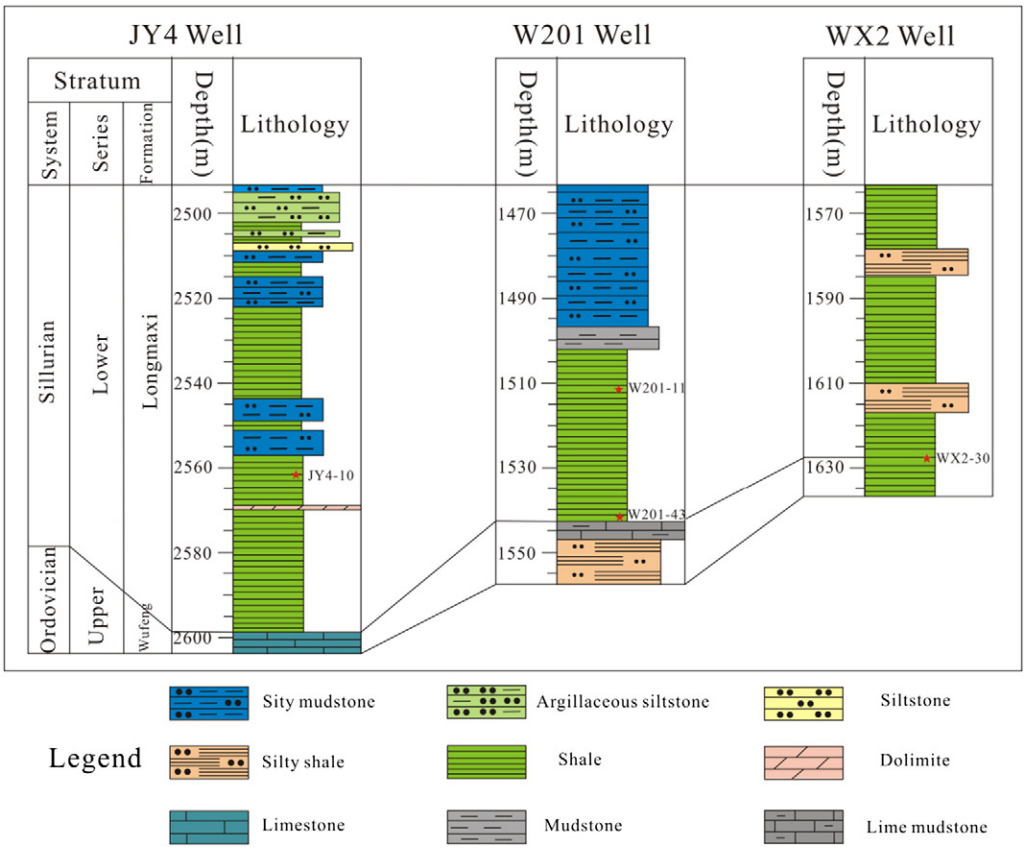

Fig. 2. Lithostratigraphic section of sampled wells (Lithology from Liang et al., 2016; Wang, 2014).

The TOC content was measured using a CS230 Elemental Analyzer (Leco Corporation, USA). About 100 mg of each sieved sample was placed in a crucible with 5% HCl and heated at 80 °C to remove carbonates. The sample was then washed six times with deionized water to remove residual HCl. The treated powder was dried and mixed with iron powder and tungsten–tin alloy. The samples were then combusted at 3000 °C using O_2 as the combustion-accelerating gas and N_2 as the carrier gas. The TOC content was calculated from the peak area of CO_2 generated by combustion of the organic matter.

A small portion (10 mg) of each sieved sample was further ground to pass through 100 mesh, and then its mineral composition was determined by X-Ray diffraction (Olympus BTX II), using a Fe_2O_3 filter and Co K-alpha radiation ($\lambda = 0.179$ nm). A scan rate of 6 times/min and an exposure time of 10 s/times were used for recording the XRD traces. The mineral content was semi-quantitatively determined, based on the intensity of specific reflections, the density, and the mass absorption coefficient of the identified mineral phases.

After that Pearson correlation analysis was carried out in SPSS version 19.0 to determine the correlations between TOC or clay content and the pore systems of the four shale samples.

Table 1
Mass proportion of the shale fractions with all ranges of particle sizes.

Sample ID		Total mess (g)	Particle size range (mesh)	Mass fraction (%)
JY4-10	JY4-10-0	4.56	<60	3.07
	JY4-10-1		60–80	20.83
	JY4-10-2		80–100	17.98
	JY4-10-3		100–120	12.28
	JY4-10-4		120–140	15.35
	JY4-10-5		140–200	28.73
	JY4-10-6		>200	1.75
W201-11	W201-11-0	4.9	<60	3.06
	W201-11-1		60–80	28.78
	W201-11-2		80–100	16.53
	W201-11-3		100–120	17.96
	W201-11-4		120–140	17.96
	W201-11-5		140–200	15.31
	W201-11-6		>200	0.41
W201-43	W201-43-0	6.26	<60	2.88
	W201-43-1		60–80	11.66
	W201-43-2		80–100	13.10
	W201-43-3		100–120	7.99
	W201-43-4		120–140	19.17
	W201-43-5		140–200	43.45
	W201-43-6		>200	1.76
WX2-30	WX2-30-0	8.69	<60	28.45
	WX2-30-1		60–80	13.45
	WX2-30-2		80–100	11.32
	WX2-30-3		100–120	14.25
	WX2-30-4		120–140	5.68
	WX2-30-5		140–200	16.82
	WX2-30-6		>200	10.02

2.3. Low-pressure CO_2 and N_2 adsorption

Low-pressure N_2 and CO_2 gas adsorption measurements were conducted using a surface area and porosimetry analyzer (Micromeritics ASAP-2460). To remove the gas, free water, and any other possible hydrocarbons, samples were automatically degassed at 110 °C using a sample degas system (Micromeritics VacPrep 061) for ~12 h prior to analyses with either N_2 or CO_2. The equilibrium interval (i.e., the time during which the pressure must remain stable within a small range) was 30 s for N_2 and 45 s for CO_2. The relative pressure (P/P_0) was 0.005–0.995 for N_2 adsorption and 0.00005–0.03 for CO_2 adsorption. During the CO_2 adsorption measurements, the free spaces were tested separately and input manually.

The N_2 and CO_2 adsorption isotherms were automatically generated by the instrument's computer. The surface areas, pore volumes, pore

Table 2
TOC content and mineral content of reference samples.

TOC range	Lithology	Sample ID	Particle size range (mesh)	TOC (%)	Minerals (%)						
						Clay		Carbonate			
					Quartz	Illite	Chlorite	Dolomite	Calcite	Albite	Pyrite
Low	Carbonaceous shale	W201-11-1	60–80	1.05	28.0	29.8	6.0	8.2	21.0	3.2	3.9
		W201-11-2	80–100	1.01	27.3	34.0	6.6	7.0	17.4	3.3	4.4
		W201-11-3	100–120	1.17	25.6	34.0	7.5	7.0	16.2	5.5	4.2
		W201-11-4	120–140	1.2	27.2	31.3	7.3	7.0	17.4	5.3	4.5
		W201-11-5	140–200	1.17	27.3	26.5	8.8	8.5	18.3	4.0	6.4
Medium	Rich clay siliceous shale	JY4-10-1	60–80	2.77	49.0	26.0	5.2	3.4	5.9	8.1	2.3
		JY4-10-2	80–100	2.98	44.4	31.2	4.8	2.2	6.1	8.5	3.0
		JY4-10-3	100–120	3.04	41.6	32.6	6.4	3.0	4.9	8.0	3.5
		JY4-10-4	120–140	3.16	44.0	30.9	4.6	3.9	6.0	7.5	3.1
		JY4-10-5	140–200	3.22	46.6	28.9	4.4	2.6	6.3	7.9	3.3
High	Lean clay siliceous shale	W201-43-1	60–80	5.23	80.3	3.0	2.1	4.4	6.4	1.9	1.9
		W201-43-2	80–100	5.62	68.8	9.3	4.6	4.5	7.1	2.5	3.2
		W201-43-3	100–120	5.66	74.3	7.9	2.4	4.1	6.3	2.7	2.3
		W201-43-4	120–140	5.75	75.8	6.7	2.0	5.3	6.5	1.8	1.8
		W201-43-5	140–200	5.81	75.1	6.7	2.0	5.0	7.7	1.8	1.8
	Rich clay siliceous shale	WX2-30-1	60–80	6.77	55.8	24.4	2.1	3.1	2.9	9.2	2.6
		WX2-30-2	80–100	6.72	51.9	26.2	3.6	2.8	3.6	8.8	3.1
		WX2-30-3	100–120	6.84	49.2	26.1	4	3.6	4.2	9.4	3.5
		WX2-30-4	120–140	6.62	57.1	20.2	3.1	3.8	3.5	9.6	2.7
		WX2-30-5	140–200	6.95	54.9	24.3	1.5	3	3.6	9.1	3.5

sizes, and PSDs were then automatically calculated based on various adsorption theories. For example, the N_2 data for the mesopore size and some of the macropore-size distributions were interpreted using the Brunauer–Emmett–Teller (BET) (Brunauer et al., 1938) and Barrett–Joyner–Halenda (BJH) (Barrett et al., 1951) methods. The CO_2 adsorption data were interpreted using the Dubinin–Astakhov (D–A) and Dubinin–Radushkevich (D–R) models. These methods were comprehensively discussed by Gregg and Sing (1991). The pore size distribution was determined by the non-local density functional theory (NLDFT; Vishnyakov et al., 1999). The total surface areas (~0.33–100 nm) and total pore volumes (~0.33–100 nm) of nanopore were interpreted using the composited N_2 and CO_2 NLDFT method (Wei et al., 2016).

3. Results

3.1. TOC and XRD analyses

The results of the analyses, including the TOC content and the mineral composition of the different particle-size ranges of the four shale samples, are presented in Table 2. The samples with a smaller

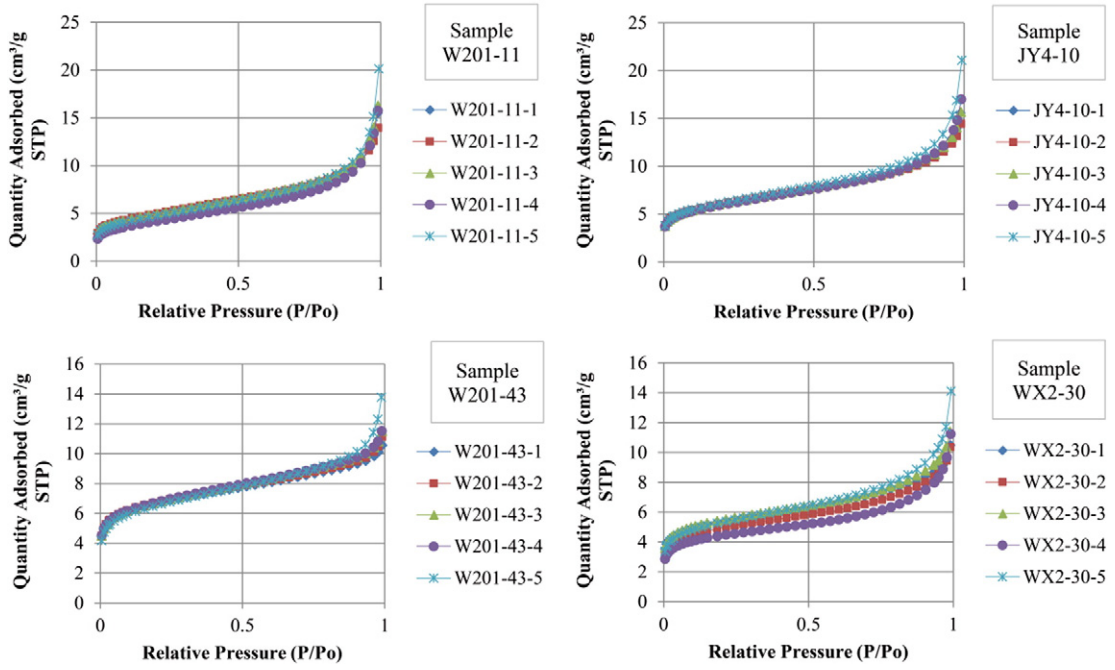

Fig. 3. Nitrogen isotherms collected of the different mesh ranges of four shale samples.

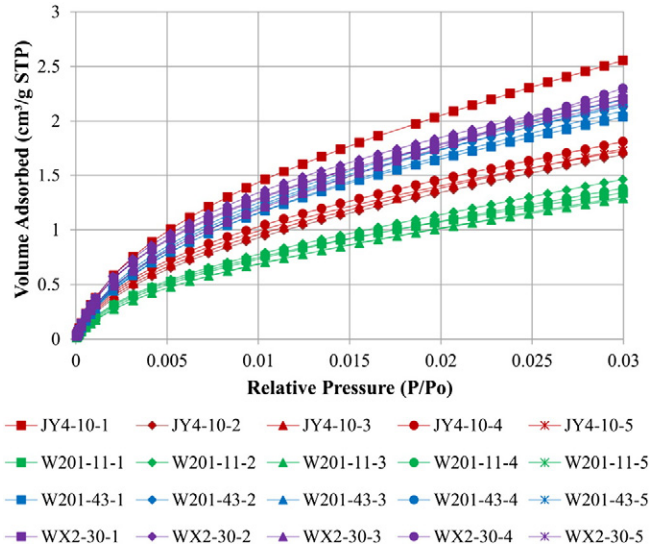

Fig. 4. Carbon dioxide isotherms collected of the different mesh ranges of four shale samples.

particle size were relatively enriched with organic matter and showed irregular variations in mineral content.

3.2. N_2 and CO_2 adsorption

As demonstrated previously (Clarkson et al., 2013), CO_2 adsorption at 0 °C can be used to estimate micropore (<2 nm) volume, and N_2 adsorption at −196 °C can be used to estimate the pore volume in the larger mesopore (2–50 nm) to macropore (>50 nm) range. Therefore, the combination of CO_2 and N_2 adsorption data covers a wide range in micro- to macroporosity up to a limit of <100 nm.

The adsorption branch data show that N_2 adsorption isotherms (Fig. 3) are Type II according to the IUPAC classification (2015) (Thommes et al., 2015) indicative of multi-layer adsorption, and they can be interpreted using the BET and BJH theories. CO_2 adsorption isotherms (Fig. 4) are Type I, indicative of microporous solids, and can be interpreted by the D-R and D-A methods. All the samples exhibit similar isotherm shapes.

As obtained from N_2 adsorption analysis, a wide variation in BET surface areas, BJH pore volumes, and BET pore sizes for the different particle-size ranges was easily observed (Table 3). A clear variation in D-R micropore surface areas and D-A micropore volumes was also observed, as determined from CO_2 adsorption analysis (Table 3). The NLDFT total surface areas (~0.33–100 nm) and total pore volumes (~0.33–100 nm) of nanopore were obtained in Table 3 too.

Table 3
Pore structure parameters (surface areas, pore volumes and pore sizes) of shale samples.

Sample ID	Particle size range (mesh)	N_2			CO_2		$N_2 + CO_2$	
		S_{BET} (m^2/g)	V_{BJH} (10^{-3} cm^3/g)	D_{BET} (nm)	S_{D-R} (m^2/g)	V_{D-A} (10^{-3} cm^3/g)	S_{NLDFT} (m^2/g)	V_{NLDFT} (10^{-3} cm^3/g)
JY4-10	60–80	21.70	18.45	4.43	14.26	7.95	23.43	22.79
	80–100	21.99	16.54	4.06	13.99	7.17	23.43	21.00
	100–120	21.83	18.78	4.40	14.14	7.28	23.55	22.90
	120–140	21.55	17.30	4.79	14.39	7.96	23.92	24.79
	140–200	22.34	27.30	5.84	14.02	7.07	24.13	30.45
W201-11	60–80	17.15	20.31	5.52	10.69	6.33	18.41	22.78
	80–100	17.64	17.65	4.69	10.95	6.41	19.11	20.41
	100–120	17.39	21.55	5.67	10.50	6.57	18.12	23.80
	120–140	15.69	21.66	6.52	10.98	7.55	15.48	23.22
	140–200	16.74	27.88	6.94	10.35	7.39	17.71	28.61
W201-43	60–80	23.98	7.80	2.69	16.82	9.71	26.93	15.18
	80–100	24.43	8.19	2.78	17.84	10.06	27.76	16.00
	100–120	24.40	8.98	2.87	17.80	9.98	27.36	16.53
	120–140	24.67	9.27	2.94	18.32	9.16	27.91	17.12
	140–200	23.60	14.18	3.61	18.26	10.10	27.33	20.11
WX2-30	60–80	19.48	8.56	3.30	18.21	8.41	25.37	15.36
	80–100	18.09	9.15	3.52	17.82	8.24	23.62	15.34
	100–120	19.63	11.80	3.62	18.05	8.14	25.36	16.95
	120–140	17.11	9.88	4.22	18.49	8.65	22.75	16.52
	140–200	19.15	16.38	4.40	17.44	7.99	24.43	20.58

S_{BET}: BET surface area.
V_{BJH}: BJH adsorption cumulative volume.
D_{BET}: BET adsorption average pore diameter.
S_{D-R}: Micropore surface area by D-R method.
V_{D-A}: Limiting micropore volume by D-A method.
S_{NLDFT}: Total surface area (0.33–100 nm) by the composited N_2 and CO_2 NLDFT method.
V_{NLDFT}: Total pore volume (0.33–100 nm) by the composited N_2 and CO_2 NLDFT method.

Table 4
Pearson correlation analyses between TOC/illite content and pore structure parameters of reference samples.

Sample ID	Pearson correlation analyses		S_{BET}	V_{BJH}	D_{BET}	S_{D-R}	V_{D-A}	S_{NLDFT}	V_{NLDFT}
JY4-10	TOC	Pearson correlation	−0.04	0.39	0.60	0.39	−0.15	0.75	0.55
		Sig. (2-tailed)	0.94	0.51	0.29	0.52	0.81	0.15	0.33
	Illite content	Pearson correlation	−0.46	−0.83	−0.88*	−0.01	0.06	−0.70	−0.86
		Sig. (2-tailed)	0.43	0.08	0.05	0.99	0.92	0.19	0.06
W201-11	TOC	Pearson correlation	−0.56	0.65	0.70	−0.21	0.80	−0.64	0.61
		Sig. (2-tailed)	0.33	0.23	0.19	0.73	0.10	0.25	0.28
	Illite content	Pearson correlation	0.29	−0.17	−0.13	0.17	0.06	−0.01	−0.19
		Sig. (2-tailed)	0.63	0.79	0.84	0.79	0.92	0.99	0.76
W201-43	TOC	Pearson correlation	0.11	0.64	0.68	0.98**	0.04	0.67	0.76
		Sig. (2-tailed)	0.86	0.24	0.21	0.00	0.94	0.22	0.14
	Illite content	Pearson correlation	0.42	0.09	0.13	0.66	0.34	0.72	0.20
		Sig. (2-tailed)	0.49	0.88	0.84	0.22	0.58	0.17	0.74
WX2-30	TOC	Pearson correlation	0.75	0.73	0.19	−0.82	−0.92*	0.54	0.80
		Sig. (2-tailed)	0.14	0.16	0.76	0.09	0.03	0.35	0.10
	Illite content	Pearson correlation	0.45	−0.03	−0.57	−0.57	−0.74	0.40	0.13
		Sig. (2-tailed)	0.45	0.97	0.31	0.31	0.15	0.51	0.84

** Correlation is significant at the 0.01 level (2-tailed).
* Correlation is significant at the 0.05 level (2-tailed).

4. Discussion

4.1. Effect of sieving on TOC and mineral contents

The adsorption properties of shale are mainly influenced by organic matter and clay minerals. Many studies have examined gas adsorption by organic matter in shale, revealing a positive correlation between organic matter content and the adsorption capacity of raw shale samples (Lu et al., 1995; Cui et al., 2009). In addition, clay minerals especially the illite contents have a strong influence on gas adsorption by shale (Jin and Firoozabadia, 2013; Ma et al., 2015).

Pearson correlation analysis (using the software SPSS 19.0) was used to determine the correlations between TOC or illite content and the pore systems of the four shales (Tables 4). We found no significant correlations between the TOC content and pore structure parameters, except that the correlation of D-R micropore surface area of sample W201-43 is significant at the 0.01 level (2-tailed) and the correlation of D-A micropore volume of sample WX2-30 is significant at the 0.05 level (2-tailed). Furthermore, there were no significant correlations between illite content and the pore structure parameters, Therefore, variations in organic matter content and mineral composition caused by sieving are probably not an important influence on the pore structure characteristics of shales. Rather, particle size is the most important control identified in this study.

Table 5
Relative standard deviations of pore structure parameters of reference samples.

Sample ID	Particle size range	Relative standard deviation (%)						
		S_{BET}	V_{BJH}	D_{BET}	S_{D-R}	V_{D-A}	S_{NLDFT}	V_{NLDFT}
JY4-10	60–200	1.39	22.14	14.56	1.18	4.91	1.34	14.98
	60–140	0.86	**5.83**	6.71	1.20	4.49	0.98	5.25
	60–120	0.66	6.75	**4.80**	0.96	4.58	0.29	5.08
	60–100	0.94	7.73	6.17	1.36	4.45	0.02	5.78
W201-11	60–200	2.41	17.23	15.03	2.58	4.52	3.51	12.62
	60–140	2.36	**9.19**	13.35	2.11	1.79	3.69	**6.60**
	60–120	1.40	10.06	**9.93**	2.11	1.89	2.75	7.79
	60–100	1.98	9.94	11.49	1.73	0.93	2.65	7.76
W201-43	60–200	1.74	26.66	12.20	3.38	3.98	1.41	11.10
	60–140	2.27	**2.45**	1.71	2.07	5.99	1.41	2.57
	60–120	1.03	7.19	3.31	3.31	1.86	1.52	4.28
	60–100	1.31	3.43	2.41	4.17	2.52	2.15	3.72
WX2-30	60–200	3.69	29.16	12.39	2.21	3.08	3.17	12.05
	60–140	4.13	**6.42**	10.73	1.54	2.68	3.65	4.10
	60–120	4.17	6.90	**4.63**	1.09	1.67	3.78	4.95
	60–100	4.13	7.00	4.55	1.53	1.45	4.21	4.37

In a set of sample parameters which almost all of the RSD values were >5%, the value in bold means the minimum RSD values for choosing.

4.2. Effect of particle size on N_2 low-pressure adsorption measurements

The N_2 adsorption analyses reveal a wide variation in the parameters of the pore systems (Table 5). The relative standard deviations (RSDs) of the BET surface areas in the different particle-size ranges of the four shales are <5%, within the analytical error. This result indicates that particle size for 60–200 mesh has no significant effect on BET surface areas calculated from N_2 low-pressure adsorption measurements. However, there was a significant difference in the RSDs of the BJH pore volumes and BET pore sizes of the samples in the 60–200 mesh range (Table 5), for which almost all of the RSD values were >5%. The minimum RSD values for four samples of V_{BJH} were obtained mainly in the 60–140 mesh particle size, which indicates that this range could be used for statistical analysis. However, the minimum RSD values for samples of D_{BET} were obtained mainly in the 60–120 mesh range. After studying the measured experimental results of BET pore sizes, we found only the data of 140–200 mesh samples are significantly larger than other mesh ranges. Therefore, a 60–140 mesh size of D_{BET} values may be used for statistical analysis. In summary, the RSD values indicate that the 60–140 mesh particle-size range is suitable for use in N_2 low-pressure adsorption measurements.

4.3. Effect of particle size on CO_2 low-pressure adsorption measurements

The results of the CO_2 adsorption analysis highlight several important variations in pore system parameters with particle size (Table 5). The RSDs of the D-R micropore surface areas and D-A micropore volumes in the different particle-size ranges were <5%, which indicates that sample particle size had no significant effect on micropore surface area and micropore volumes in the 60–200 mesh grain size in the CO_2 low-pressure adsorption analysis. Therefore, the 60–200 mesh particle size range is suitable for use in CO_2 low-pressure adsorption measurements.

4.4. Effect of particle size on the composited N_2 and CO_2 low-pressure adsorption measurements

The RSDs of total surface areas and total pore volumes of nanopore were interpreted using the composited N_2 and CO_2 NLDFT method with different particle size were obtained in Table 5. The RSDs of the S_{NLDFT} in the different particle-size ranges were <5%, which indicates that sample particle size had no significant effect on nanopore surface area in the 60–200 mesh grain size in the composited N_2 and CO_2 analysis. The RSDs of the V_{NLDFT} of 140–200 mesh range are significantly larger than other mesh ranges which are smaller than 5% or a little

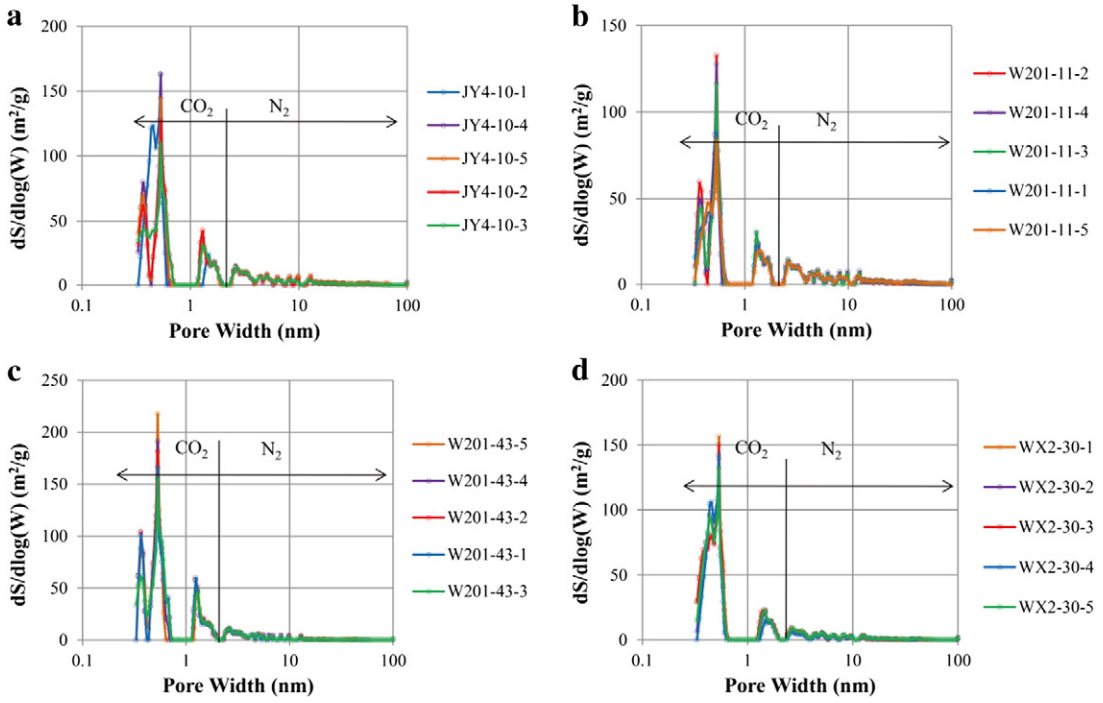

Fig. 5. Combined nitrogen and carbon dioxide specific surface area distributions (dS/dlogW plots) (arrows indicate range of pore sizes covered by N_2 and CO_2 adsorption).

larger than 5%. Therefore, the 60–140 mesh particle size range is suitable for use in the composited N_2 and CO_2 analysis.

4.5. Effect of pore size distribution on N_2/CO_2 low-pressure adsorption

The dS/dlogW (Surface Area vs. Pore Width) and dV/dlogW (Pore Volume vs. Pore Width) plots for N_2 and CO_2 can generally be used to estimate the pore size distribution of N_2/CO_2 low-pressure adsorption. In such plots, CO_2 and N_2 curves start and end at 2 nm, respectively, and show a near seamless transition (Figs. 5 and 6). The N_2 dS/dlogW plots show just a single clear peak (Fig. 5) in the shale pore structure, and all the samples show similar characteristics in the N_2 dS/dlogW plots. The N_2 dV/dlogW plots indicate the shale pore structure is multi-modal (Fig. 6). A marked change (high N_2 peaks and new N_2 peaks) appeared in the 10–100 nm pore-width range, particularly for samples in the 140–200 mesh range, which are much higher than other mesh ranges (the yellow lines in Fig. 6a–d). This finding indicates that sample with smaller particle sizes have a greater effect on determination of the pore-size distribution N_2 adsorption. This effect increases with increasing sample mass.

The CO_2 dS/dlogW and dV/dlogW plots indicate multi-modal PSDs (~0.5 nm and 1.5 nm) in the micropore range (<2 nm) (Figs. 5 and 6).

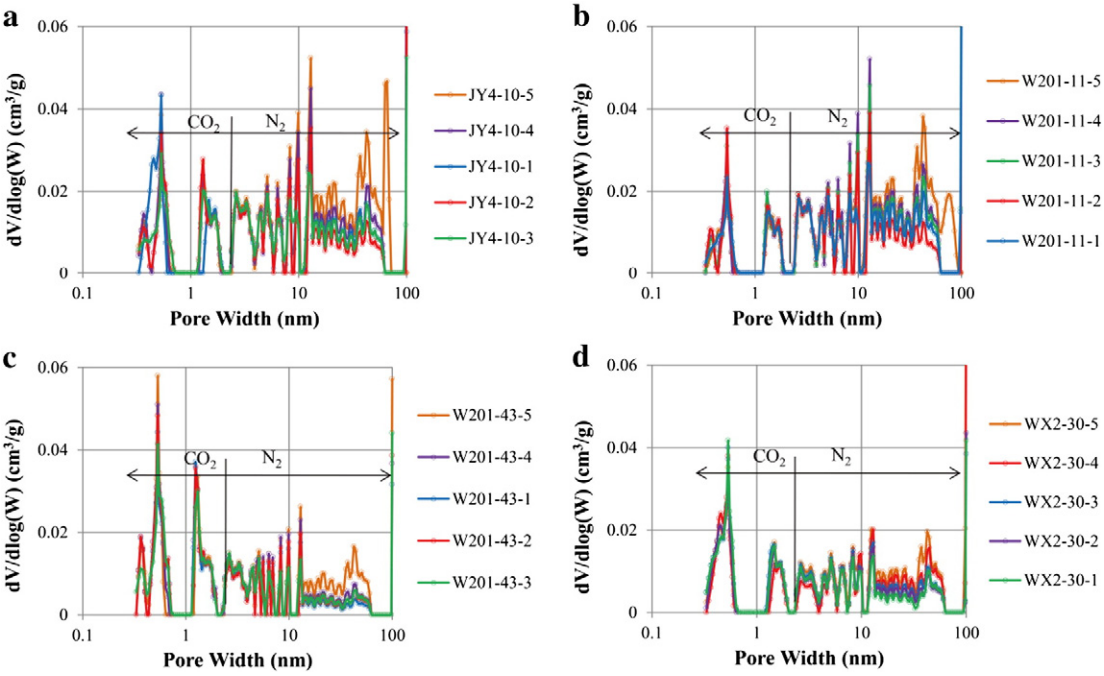

Fig. 6. Combined nitrogen and carbon dioxide pore volume distributions (dV/dlogW plots) (arrows indicate range of pore sizes covered by N_2 and CO_2 adsorption).

All the samples exhibited similar characteristics in the different particle size ranges in the CO_2 dS/dlogW and dV/dlogW plots, which suggest that sample particle size had no significant influence on the pore-size distribution estimated from CO_2 adsorption analysis.

5. Conclusion

The results show that the combination of low-pressure N_2 and CO_2 adsorption is an effective approach for characterizing the pore structure of shales. From the analysis of the effect of sample particle size on N_2 and CO_2 low-pressure adsorption measurements, the main conclusions are as follows.

(1) Samples with smaller particle size are slightly enriched in organic matter and show irregular variations in their mineral content compared with samples with larger particle sizes. However, Pearson correlation analyses showed no significant correlations between the TOC or illite contents and pore structure parameters (e.g., surface area) in the different particle-size ranges. Therefore, variations in the organic matter content and mineral composition that result from sieving are unlikely to have a significant influence on the pore structure characteristics of shale.
(2) The RSDs of the BET surface areas, D-R micropore surface areas and NLDFT nanopore surface areas measurements are <5%, within analytical error. This indicates that particle size shows insignificant effects on surface area results in the studied grain size range (60–200 mesh). Most of the RSDs of the BJH pore volumes were >5%, of which the minimum RSD values were obtained for the 60–140 mesh particle-size range. This result indicates that the 60–140 mesh particle-size range is suitable for use in N_2 low-pressure adsorption.
(3) A smaller sample particle size has a greater effect on N_2 low-pressure adsorption measurements than a larger particle size. High N_2 peaks and new N_2 peaks appeared in the 10–100 nm pore-width range, particularly for samples in the >140 mesh range. Therefore, the comprehensive analysis of RSD values of pore structure parameters and PSDs, and practical applications of the data, show that the 60–140 mesh particle size range is suitable for N_2 low-pressure adsorption measurements.
(4) The RSDs of the D-R micropore surface areas and D-A micropore volumes for the different particle-size ranges of the four shales, as determined from CO_2 adsorption analyses, were <5%. This indicates that sample particle size has no significant effect on surface area or pore volume in the 60–200 mesh grain-size range for CO_2 low-pressure adsorption measurements. Moreover, there were no obvious differences in CO_2 dS/dlogW and dV/dlogW plots of the PSD analysis. Therefore, sample particle size has no significant effect on the pore system parameters of the 60–200 mesh grain size for CO_2 low-pressure adsorption measurements.
(5) The 60–140 mesh particle-size range is suitable for use in measurements of the composited N_2 and CO_2 low-pressure adsorption.

Acknowledgements

The authors would like to acknowledge Xiao Yang and Xiulian Yao for their help during TOC and XRD experiments. And this research was financially supported by Special Fund for Strategic Priority Research Program of the Chinese Academy of Sciences (Class B) under agreement No. XDB10010500 and the GIGCAS 135 Project "135TP201602". We are grateful to editor Cevat Ozgen Karacan and anonymous reviewer for their instructive comments and suggestions that significantly help clarify this manuscript. This is contribution No. IS-2276 from GIGCAS.

References

Barrett, E.P., Johner, L.S., Halenda, P.P.J., 1951. Am. Chem. Soc. 73, 373–380.
Bruant, R.G., Guswa, A.J., Celia, M.A., Peters, C.A., 2002. Safe storage of CO_2 in deep saline aquifers. Environ. Sci. Technol. 36 (11), 240A–245A.
Brunauer, S., Emmett, P.H., Teller, E., 1938. J. Am. Chem. Soc. 60, 309–319.
Busch, A., Alles, S., Gensterblum, Y., 2008. Carbon dioxide storage potential of shales. Int. J. Greenh. Gas Control 2, 297–308.
Cao, T.T., Song, Z.G., Wang, S.B., Cao, X.X., Li, Y., Xia, J., 2015. Characterizing the pore structure in the Silurian and Permian shales ofthe Sichuan Basin, China. Mar. Pet. Geol. 61, 140–150.
Chalmers, G.R.L., Bustin, R.M., 2007. The organic matter distribution and methane capacity of the Lower Cretaceous strata of Northeastern British Columbia, Canada. Int. J. Coal Geol. 70 (1), 223–239.
Chalmers, G.R., Bustin, R.M., Power, I.M., 2012. Characterization of gas shale pore systems by porosimetry, pycnometry, surface area, and field emission scanning electron microscopy/transmission electron microscopy image analyses: examples from the Barnett, Woodford, Haynesville, Marcellus, and Doig units. AAPG Bull. 96 (6), 1099–1119.
Chareonsuppanimit, P., Mohammad, S.A., Robinson Jr., R.L., Gasem, K.A.M., 2012. High-pressure adsorption of gases on shales: measurements and modeling. Int. J. Coal Geol. 95, 34–46.
Chen, J., Xiao, X.M., 2014. Evolution of nanoporosity in organic-rich shales during thermal maturation. Fuel 129, 173–181.
Clarkson, C.R., Jensen, J.L., Pedersen, P.K., Freeman, M., 2012. Innovative methods for flow-unit and pore-structure analyses in a tight siltstone and shale gas reservoir. AAPG Bull. 96 (2), 355–374.
Clarkson, C.R., Solano, N., Bustin, R.M., Bustin, A.M.M., Chalmers, G.R.L., Hec, L., Melnichenko, Y.B., Radliński, A.P., Blach, T.P., 2013. Pore structure characterization of North American shale gas reservoirs using USANS/SANS, gas adsorption, and mercury intrusion. Fuel 103, 606–616.
Cui, X., Bustin, A.M.M., Bustin, R.M., 2009. Measurements of gas permeability and diffusivity of tight reservoir rocks: different approaches and their applications. Geofluids 9 (3), 208–223.
Curtis, J.B., 2002. Fractured shale-gas systems. AAPG Bull. 86 (11), 1921–1938.
Gregg, S.J., Sing, K.S.W., 1991. Adsorption Surface Area and Porosity. Academic Press, New York.
Guo, H.J., Jia, W.L., Peng, P., Lei, Y.H., Luo, X.R., Cheng, M., Wang, X.Z., Zhang, L.X., Jiang, C.F., 2014. The composition and its impact on the methane sorption of lacustrine shales from the Upper Triassic Yanchang Formation, Ordos Basin, China. Mar. Pet. Geol. 57, 509–520.
Han, S.B., Zhang, J.C., Li, Y.X., Horsfield, B., Tang, X., Jiang, W.L., Chen, Q., 2013. Evaluation of Lower Cambrian Shale in Northern Guizhou Province, South China: implications for shale gas potential. Energy Fuel 27, 2933–2941.
Hou, Y.G., Sheng, H.E., Yi, J.Z., Zhang, B.Q., Chen, X.H., Wang, Y., Zhang, J.K., Cheng, C.Y., 2014. Effect of pore structure on methane sorption potential of shales. Pet. Explor. Dev. 41 (2), 272–281.
Ji, L.M., Zhang, T.W., Milliken, K.L., Qu, J.L., Zhang, X.L., 2012. Experimental investigation of main controls to methane adsorption in clay-rich rocks. Appl. Geochem. 27, 2533–2545.
Jiang, C.L., Séquaris, J.M., Wacha, A., Bóta, A., Vereecken, H., Klumppa, E., 2014. Effect of metal oxide on surface area and pore size of water-dispersible colloids from three German silt loam topsoils. Geoderma 235–236, 260–270.
Jin, Z.H., Firoozabadia, A., 2013. Methane and carbon dioxide adsorption in clay-like slit pores by Monte Carlo simulations. Fluid Phase Equilib. 360, 456–465.
Labani, M.M., Rezaee, R., Saeedi, A., Hinai, A.A., 2013. Evaluation of pore size spectrum of gas shale reservoirs using low pressure nitrogen adsorption, gas expansion and mercury porosimetry: a case study from the Perth and Canning Basins, Western Australia. J. Pet. Sci. Eng. 112, 7–16.
Lahann, R., Mastalerz, M., Rupp, J.A., Drobniak, A., 2013. Influence of CO_2 on New Albany Shale composition and pore structure. Int. J. Coal Geol. 108, 2–9.
Li, Y.J., Li, X.Y., Wang, Y.L., Yu, Q.C., 2015. Effects of composition and pore structure on the reservoir gas capacity of Carboniferous shale from Qaidam Basin, China. Mar. Pet. Geol. 62, 44–57.
Liang, F., Bai, W.h., Zou, C.n., Wang, H.Y., Wu, J., Ma, C., Zhang, Q., Guo, W., Sun, S.S., Zhu, Y.M., Cui, H.Y., Liu, D.X., 2016. Shale gas enrichment pattern and exploration significance of Well Wuxi-2 in northeast Chongqing, NE Sichuan Basin. Pet. Explor. Dev. 3, 350–359.
Liu, D., Peng, Y.N., Liu, H.M., Li, T., Tan, D.Y., Yuan, W.W., He, H.P., 2013. High-pressure adsorption of methane on montmorillonite, kaolinite and illite. Appl. Clay Sci. 85, 25–30.
Lu, X.C., Li, F.C., Watson, A.T., 1995. Adsorption measurements in Devonian shales. Fuel 74 (4), 599–603.
Ma, Y., Zhong, N.N., Li, D.H., Pan, Z.J., Cheng, L.J., Liu, K.Y., 2015. Organic matter/clay mineral intergranular pores in the Lower Cambrian Lujiaping Shale in the north-eastern part of the upper Yangtze area, China: a possible microscopic mechanism for gas preservation. Int. J. Coal Geol. 137, 38–54.
Mastalerz, M., Schimmelmann, A., Drobniak, A., Chen, Y.Y., 2013. Porosity of Devonian and Mississippian New Albany Shale across a maturation gradient: insights from organic petrology, gas adsorption, and mercury intrusion. AAPG Bull. 97 (10), 1621–1643.
Ross, D.J., Bustin, R.M., 2007. Impact of mass balance calculations on adsorption capacities in microporous shale gas reservoirs. Fuel 86 (17), 2696–2706.
Ross, D.J., Bustin, R.M., 2009. The importance of shale composition and pore structure upon gas storage potential of shale gas reservoirs. Mar. Pet. Geol. 26 (6), 916–927.
Tan, J.Q., Horsfield, B., Mahlstedt, N., Zhang, J.C., Primio, R., Vu, T.A.T., Boreham, C.J., Graas, G., Tocher, B.A., 2013. Physical properties of petroleum formed during maturation of Lower Cambrian shale in the upper Yangtze Platform, South China, as inferred from PhaseKinetics modeling. Mar. Pet. Geol. 48, 47–56.

Tan, J.Q., Weniger, P., Krooss, B., Merkel, A., Horsfield, B., Zhang, J.C., Boreham, C.J., Graas, G., Tocher, B.A., 2014a. Shale gas potential of the major marine shale formations in the Upper Yangtze Platform, South China, part II: Methane sorption capacity. Fuel 129, 204–218.

Tan, J.Q., Horsfield, B., Fink, R., Krooss, B., Schulz, H., Rybacki, E., Zhang, J.C., Boreham, C.J., Graas, G., Tocher, B.A., 2014b. Shale gas potential of the major marine shale formations in the Upper Yangtze Platform, South China, part III: mineralogical, lithofacial, petrophysical, and rock mechanical properties. Energy Fuel 28, 2322–2342.

Tan, J.Q., Horsfield, B., Mahlstedt, N., Zhang, J.C., Boreham, C.J., Hippler, D., Graas, G., Tocher, B.A., 2015. Natural gas potential of Neoproterozoic and lower Palaeozoic marine shales in the Upper Yangtze Platform, South China: geological and organic geochemical characterization. Int. Geol. Rev. 57, 305–326.

Thommes, M., Kaneko, K., Neimark, A.V., Olivier, J.P., Rodriguez-Reinoso, F., Rouquerol, J., Sing, K.S.W., 2015. Physisorption of gases, with special reference to the evaluation of surface area and pore size distribution (IUPAC technical report). Pure Appl. Chem. 87 (9–10), 1051–1069.

Tian, H., Pan, L., Xiao, X.M., Wilkins, R.W.T., Meng, Z.P., Huang, B.J., 2013. A preliminary study on the pore characterization of Lower Silurian black shales in the Chuandong Thrust Fold Belt, southwestern China using low pressure N_2 adsorption and FE-SEM methods. Mar. Pet. Geol. 48, 8–19.

Tian, H., Pan, L., Zhang, T.W., Xiao, X.M., Meng, Z.P., Huang, B.J., 2015. Pore characterization of organic-rich Lower Cambrian shales in Qiannan Depression of Guizhou Province, Southwestern China. Mar. Pet. Geol. 62, 28–43.

Tsai, W.T., 2013. Microstructural characterization of calcite-based powder materials prepared by planetary ball milling. Materials 6, 3361–3372.

Vishnyakov, A., Ravikovitch, P.I., Neimark, A.V., 1999. Molecular level models for CO_2 sorption in nanopores. Langmuir 15, 8736–8742.

Wang, Z.G., 2014. Practice and cognition of shale gas horizontal well fracturing stimulation in Jiaoshiba of Fuling area. Oil Gas Geol. 35 (3), 425–430 (In Chinese with English abstract).

Wang, S.B., Song, Z.G., Cao, T.T., Song, X., 2013. The methane sorption capacity of Paleozoic shales from the Sichuan Basin, China. Mar. Pet. Geol. 44, 112–119.

Wang, Y., Zhu, Y.M., Chen, S.B., Li, W., 2014. Characteristics of the Nanoscale pore structure in northwestern Hunan shale gas reservoirs using field emission scanning electron microscopy, high-pressure mercury intrusion, and gas adsorption. Energy Fuel 28 (2), 945–955.

Wei, M.M., Zhang, L., Xiong, Y.Q., Li, J.H., Peng, P., 2016. Nanopore structure characterization for organic-rich shale using the non-local-density functional theory by a combination of N_2 and CO_2 adsorption. Microporous Mesoporous Mater. 227, 88–94.

Yang, F., Ning, Z.F., Liu, H.Q., 2014. Fractal characteristics of shales from a shale gas reservoir in the Sichuan Basin, China. Fuel 115, 378–384.

Yuan, W.N., Pan, Z.J., Li, X., Yang, Y.X., Zhao, C.X., Connell, L.D., Li, S.D., He, J.M., 2014. Experimental study and modelling of methane adsorption and diffusion in shale. Fuel 117, 509–519.

Zelenev, A.S., Champagne, L.M., Hamilton, M., 2011. Investigation of interactions of diluted microemulsions with shale rock and sand by adsorption and wettability measurements. Colloids Surf. A Physicochem. Eng. Asp. 391, 201–207.